Journal of Applied Polymer Science

Electrostatic Deposition of Silica Nanoparticles between E-Glass Fibers and an Epoxy Resin

Benjamin H. Rutz, John C. Berg
Department of Chemical Engineering, Box 351750, University of Washington, Seattle, Washington 98195
Correspondence to: J. C. Berg (E-mail: berg@cheme.washington.edu)

ABSTRACT: The achievement of optimum adhesion between a thermoset and an inorganic material is an important goal for the composites and coatings industries. There is a growing interest in the use of structural surface modifiers, such as nanotubes, nanoparticles, and whiskers, to improve this adhesion. Here, a method for electrostatically depositing poly(ethylene imine)-functionalized silica nanoparticles onto E-glass fibers was developed. The deposition of 26-nm functionalized particles onto glycidyloxypropyltrimethoxysilane (GPS)-functionalized E-glass fibers and then their embedding in a resin of diglycidyl ether of bisphenol A and *m*-phenylene diamine increased the interfacial shear strength (IFSS) 35% over that of bare fibers and 8% over that of GPS-functionalized fibers. IFSS was highly dependent on the particle size; the 16-nm functionalized particles had little effect on the IFSS. When the particles size was increased to 71 and 100 nm, this led to increasingly poor IFSS values, whereas the 26-nm particles produced the best results. Similar results were seen with the transverse flexural strength of the unidirectional composites. © 2014 Wiley Periodicals, Inc. J. Appl. Polym. Sci. **2015**, *132*, 41516.

KEYWORDS: colloids; composites; mechanical properties; self-assembly

Received 4 June 2014; accepted 15 September 2014
DOI: 10.1002/app.41516

INTRODUCTION

Fiber-reinforced plastics (FRPs) are comprised of high-strength, high-modulus fibers embedded in a polymeric matrix. Their mechanical properties are determined not only by the fiber and matrix but also by the interphase between them. The *interphase* is the region surrounding the fiber; it has mechanical and chemical properties distinct from the bulk polymer and the fiber.[1] Adhesion must be optimized to achieve optimum mechanical properties for a given fiber–matrix system.[2,3] For glass fibers, the adhesion is often improved with silane coupling agents.[4]

Alternatively, the interphase can be modified by the introduction of whiskers, carbon nanotubes (CNTs) or particles to the fiber surface, and it has been proposed that their presence can increase mechanical interlocking and improve the adhesion. In some cases, interphase modifiers, such as whiskers of Si_3N_4, TiO_2, and SiC, have been grown directly on the surface of the carbon fibers.[5] In these cases, the interlaminar shear strengths were improved, but the in-plane properties were reduced because of the fiber damage caused by high-temperature processing. Although there has been interest in the growth of CNTs on carbon fibers with chemical vapor deposition,[6,7] the harsh environment damages the fibers and limits the feasibility of commercialization. ZnO whiskers have been grown on carbon fibers under benign reaction conditions,[8–10] and improvements in the interfacial shear strength (IFSS), lamina shear strength, and modulus were reported. The surface roughness of glass fibers has been increased by treatment with a tetraethylorthosilicate/glycidyloxypropyltrimethoxysilane (GPS) blend, with a modest increase in IFSS reported.[11]

Instead of the growth of structures on the surface of fibers, it is possible to synthesize structural interphase modifiers separately and to deposit them on the surface. CNTs have been deposited onto carbon fibers with electrophoresis,[12] whereas CNTs treated with poly(ethylene imine) (PEI) were electrostatically deposited.[13] This modestly increased IFSS. In another study, silica particles were incorporated into a sizing package with other adhesion modifiers to improve the impact energy absorption of an E-glass composite.[14,15] Our laboratory investigated the effects on the IFSS, longitudinal tensile strength, and modulus in E-glass and poly(vinyl butyral) composites of the modification of the interphase with polymeric core–shell PEI–polystyrene particles.[3] Two different particle diameters were investigated, 143 and 327 nm. The 327-nm particles led to only a modest improvement in the properties, whereas 143-nm particles increased the IFSS and longitudinal tensile modulus and strength by 56, 42, and 34%, respectively. This enhancement was attributed to both an increased effective surface area and an

increase in the modulus and toughness of the interphase. In general, with the exception of ZnO whiskers, the increase in IFSS has been uniformly modest.

It remains an open question whether significant improvements in the adhesion and composite properties can be obtained with structural interphase modifiers when factors such as the element size, modulus, spatial distribution, and degree of attachment are optimized. In this study, we developed a procedure for uniform particle deposition and attachment using electrostatics, controlled with the pH and ionic strength, and we examined, in particular, the effect of the particle size on adhesion. We investigated how trimethoxysilane-modified poly(ethylene imine) (SPEI)-functionalized silica nanoparticles electrostatically deposited to GPS-functionalized E-glass fibers affected the IFSS of a single-fiber composite and the transverse flexural strength of a unidirectional FRP made with diglycidyl ether of bisphenol A (BADGE) and *m*-phenylene diamine (mPDA), as a function of particle size from 16 to 100 nm. Sixteen-nanometer particles had no statistically significant effect on the IFSS, 26-nm particles increased the IFSS by 35% over bare fibers when used with GPS and increased the IFSS by 8% over GPS-functionalized fibers, 71-nm particles reduced the IFSS by 4%, and 100-nm particles reduced the IFSS by 27%. These results suggest the potential value in the use of functionalized mineral oxide nanoparticles as structural interphase modifiers in FRPs to improve fiber–resin adhesion and demonstrate the need for careful control of particle size.

EXPERIMENTAL

SPEI-functionalized silica nanoparticles were electrostatically deposited onto the surface of the GPS-functionalized E-glass fibers. The particle-coated fibers were embedded in a thermoset matrix and then subjected to a single-fiber fragmentation test (SFFT) to determine the IFSS and a three-point bending test to determine the transverse flexural strength and modulus.

Fiber Functionalization

E-glass fibers (Fiberex, Inc., Leduc, Alberta, Canada) were desized as tows by soaking in NoChromix (Godax Laboratories, Cabin John, MD) and concentrated sulfuric acid for 90 min. The fibers were rinsed with deionized (DI) H_2O and then dried at 100°C for several hours. The desized fibers had an average diameter of 8.9 μm, as determined by scanning electron microscopy (SEM; JSM 7000, JEOL, Akishima, Japan) image analysis. Individual fibers were removed from the tow and mounted on a handling jig. A concentration of 0.5 vol % GPS (Gelest, Inc., Morrisville, PA) was hydrolyzed in 190-proof ethanol for 20 min with sufficient acetic acid to reduce the pH to 4.5. The fibers were submerged for 60 min and then dried at room temperature. For comparison, one set of fibers was functionalized with SPEI (Gelest, Inc., number-average molecular weight = 1500–1800). The functionalization procedure was identical, except 0.5 vol % SPEI was used instead of GPS.

Nanoparticle Functionalization

Four different silica nanoparticles were used, 16-nm Ludox SM-30, 26-nm Ludox TMA (Sigma-Aldrich, St. Louis, MO), 71-nm Nexsil 85A (Nyacol, Ashland, MO), and 100-nm particles (Fiber Optic Center, New Bedford, MA). The referenced particle sizes for the three smallest silica particles were determined by dynamic light scattering (90Plus, Brookhaven Instruments Corp., Holtzville, NY). The reported diameter of the 100-nm particles was provided by the manufacturer. A concentration of 1 wt % silica nanoparticles was dispersed in DI H_2O with vigorous stirring followed by 5 min of ultrasonication with a Sonifier 250 (20 kHz, 100 W) with a cup horn attachment (Branson Ultrasonics Corp., Danbury, CT). The amount of SPEI used to functionalize each batch was 0.5 vol % or that calculated from the approximate number of moles of hydroxyl functional groups on the surface, whichever was larger. The manufacturer-reported values for the surface areas for SM-30, TMA, Nexsil 85A, and 100-nm silica were 400, 140, 55, and 6 m^2/g, respectively. With the assumption of a hydroxyl surface coverage of 5 OH/nm^2,[4] the approximate molar concentration of surface hydroxyl groups was determined. With the assumption that one SPEI molecule reacted with one hydroxyl surface group, the amount of SPEI needed for each particle type was 5.80, 2.03, 0.8, and 0.5 vol %, for the 16-, 26-, 71-, and 100-nm particles, respectively. The SPEI was added dropwise with vigorous mixing, and the pH was reduced to 4.5 with acetic acid. Flocculation occurred with the addition of SPEI, which was dispersed by sonication for 15 min (model 8848, Cole-Parmer, Vernon Hills, IL). The suspensions were mixed for an additional 45 min.

After functionalization, the 16- and 26-nm particles were dialyzed with regenerated cellulose dialysis tubing (Fisher Scientific, Waltham, MA). The suspension was dialyzed in DI H_2O until the conductivity remained constant with time, typically, for 4 days. The suspensions were diluted to 0.1 vol % solid contents in DI H_2O. The 71- and 100-nm particles were centrifuged at 7500 rpm for 15 min or 5500 rpm for 10 min, respectively. The supernatant was removed, an equivalent amount of DI H_2O was added, and the particles were redispersed and centrifuged again to rinse them. Finally, the particles were redispersed in DI H_2O and diluted to achieve a 0.1 vol % solid content.

Particle Composition Determination by Thermogravimetric Analysis (TGA)

To determine the relative amounts of SPEI and silica, the colloidal suspensions were dried at room temperature; about 20 mg of the solids were placed in an alumina crucible and heated to 900°C at 20°C/min in a TGA instrument (Q50, TA Instruments, New Castle, DE).

Particle Deposition on the Fibers

The pH range where the SPEI particles had a positive charge and the fibers had a negative charge [their respective points of zero charge (*pzc*'s) were determined with electrophoresis measurements, ZetaPALS, Brookhaven Instruments Corp, Holtzville, NY] with KOH and HNO_3 as pH modifiers. The functionalized E-glass was ground with a mortar and pestle. The optimum pH was determined by the electrostatic deposition of SPEI particles on the fibers and with SEM micrographs, it was found to be 7.0. The pH of all of the suspensions was adjusted to 7.0 with KOH and HNO_3. The opposing electrical potential caused the particles to spontaneously deposit on the surface of the fiber. However, to achieve optimum surface coverage, it was necessary

to add salt. KNO_3 was added to the suspensions at concentrations of 0.5, 0.75, 0.015, and 0.05*M* for the 16-, 26-, 71-, and 100-nm silica, respectively. The 0.1 vol % SPEI-functionalized silica suspensions were heated to 85°C, and the GPS-functionalized fibers were submerged for 60 s. The fibers were then rinsed with DI H_2O to remove any residual salt. The optimum conditions for surface coverage (KNO_3 concentration, pH, particle volume fraction, and submersion duration) were determined by the independent systematic variation of each variable followed by qualitative observation of the SEM images.

Wipe Test

To qualitatively determine the adhesion between the nanoparticles and the fiber surfaces, a wipe test was performed. After particle deposition, the fiber was placed between two 2.5 × 7.5 cm^2 pieces of Whatman 41 filter paper (Whatman International, Ltd., Springfield Mill, United Kingdom), backed by glass microscope slides and weighted to generate 690 Pa of pressure. The fiber was then pulled through the filter paper at about 1 cm/s, and the fibers were imaged with SEM to determine the extent of particle removal.

Single-Fiber Strength Determination

The strength of the E-glass fibers, as-received (sized), bare (desized), and GPS-functionalized, was determined in accordance with ASTM C1557 with a tensile testing machine (T1000, Satec, Grove City, PA). The fibers were mounted in paperboard tabs to facilitate handling. The gauge length was 5 cm, and the displacement rate was 1 mm/min. Twenty specimens of each fiber type were tested.

Single-Fiber Composite Specimen Preparation

Individual fibers were suspended across a dogbone silicone mold, with a 25.4 × 4 × 1.5 mm^3 gauge section. A stoichiometric ratio of BADGE (EP-828, Miller-Stephenson, Danbury, CT) and mPDA (Sigma-Aldrich, St. Louis, MO) were mixed for 10 min at 800 rpm at 75°C. A volume of 0.8 mL was pipetted into the mold cavities, cured at 75°C for 2 h, and postcured at 125°C for an additional 2 h.

SFFT

A dogbone sample was placed in a miniature tensile test frame (St. John's Computer Machine, St. John's, MI), and the tensile strain was applied at 0.003 mm mm^{-1} min^{-1}. Generally, fiber fragmentation started at a strain of 8% and was saturated with breaks at 10%. The samples were strained to 12%. At least six samples were tested for each system; 10 samples were typical.

The IFSS was approximated with the Kelly–Tyson model,[16] where the IFSS is the maximum shear stress (τ) and is given by

$$\tau = \frac{\sigma_{f,c} d}{2 l_c} \quad (1)$$

where $\sigma_{f,c}$ is the tensile strength of the fiber, d is the fiber diameter, and l_c is the critical fiber length, or approximately the minimum length of fiber needed to generate enough fiber axial stress to cause the fiber to break.

Flexural Properties of the Unidirectional Composites

To generate a laboratory-scale unidirectional composite from a single tow, the tow was wrapped around a rectangular frame (10 × 25 cm^2) made from a borosilicate glass rod. The location and number of wraps was carefully controlled to create dimensionally consistent specimens. Once the fibers were wrapped on the frame, they were surface-treated in the same manner as the single-fiber specimens.

The composites were made with typical vacuum-assisted resin transfer molding with EP-828 and mPDA. A vacuum of 0.9 atm was applied during resin transfer and for the first 2 h of curing to ensure good fiber compaction. The composite plates were cured for 2 h at 75°C and 2 h at 125°C. The plates were cut into 12.5 × 75 mm^2 specimens with a water-cooled abrasive saw with a thickness of 1.25 mm.

The three-point bending test was performed according to ASTM D 7264, with a span-to-thickness ratio of 32:1 and a displacement rate of 1 mm/min in a Satec mechanical test machine (T1000, Grove City, PA).

Table I. Weibull Scale Factor, Shape Factor, and Mean Values of the Sized, Desized, and GPS-Functionalized E-Glass Fibers

	Scale factor (MPa)	Shape factor	Mean (MPa)
Sized	4512	7.8	4244
Bare	3911	7.6	3681
GPS	4349	3.3	3900

RESULTS AND DISCUSSION

Fiber Strength

The strengths of the sized, desized, and GPS-functionalized E-glass fibers were determined because these values were needed to accurately determine the IFSS. Cumulative Weibull distributions were fit to the data from single-fiber strength testing for the three fiber types investigated, with the Weibull shape and scale parameters returned. From these parameters, the Weibull means could be calculated, and they are given in Table I.

The strength of ceramic fibers is largely controlled by the presence of surface flaws. To prevent the accumulation of these flaws, the fibers are coated with a sizing to protect the fibers and to improve processing. In this study, it was necessary to remove the sizing and expose the fiber to flaws introduced during handling. This invariably led to a decrease in strength. When the desized fibers were treated with GPS, they crosslinked on and with the fiber surface. This mitigated the surface flaws[17] and led to an increase in the average fiber strength compared to the desized fibers. The relatively small shape factor for the GPS-functionalized fibers was indicative of a large variation in the fiber strength and indicated that GPS strengthened the fibers inconsistently.

Surface Coverage as a Function of the pH and Salt Concentration

The targeted particle surface concentration on the fibers was near monolayer; this prevented particle–particle contact. A lower surface coverage reduced the effect of particles at the interface, and a close-packed monolayer reduced the effective surface roughness. A uniform multilayer could not be produced from a single-step electrostatic deposition with a nonaggregated

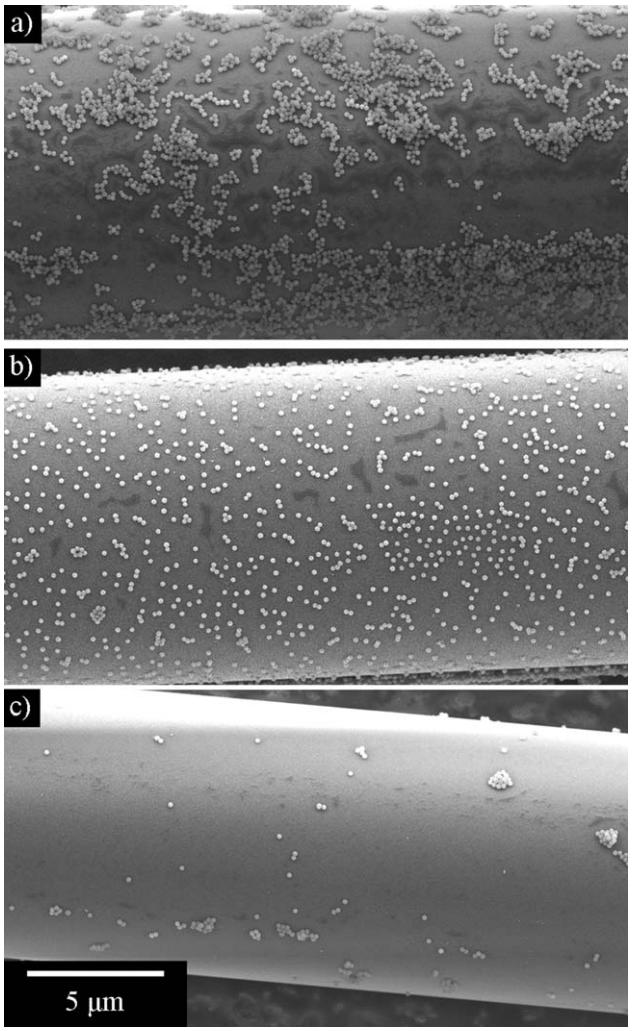

Figure 1. SPEI-functionalized, 100-nm silica particles on GPS-functionalized fibers with pHs of (a) 9.2, (b) 7.0, and (c) 4.4.

suspension because the deposited particles screened the negative fiber surface charge.

By controlling the electrostatics of the particles and fibers, it was possible to control the extent of particle coverage on the fibers. The amine groups of the SPEI caused the functionalized particles to generate a positive surface charge when the pH was lower than 10.2 (the *pzc* of the particles), and the hydroxyl groups on the E-glass fibers caused the fibers to have a negative surface charge in water when the pH was higher than 2.2 (the *pzc* of the fibers), as determined by the variation of the pH and the determination of the ζ potential. Thus, when the fibers were submerged in a suspension of SPEI-functionalized particles, they spontaneously adhered to the fiber surface. To determine the optimum pH, GPS-functionalized fibers were dipped in 0.1 vol %, 100-nm, SPEI-functionalized silica suspensions with pHs of 4.4–9.2, and the surfaces were imaged with SEM. Representative micrographs are shown in Figure 1. A pH of 7 gave the best surface coverage.

Adjusting the pH was not sufficient for obtaining a near monolayer of particles. Figure 1(b) shows the large interparticle spacing on the fiber surface. This large spacing was caused by the electrostatic repulsion between particles, which prevented the deposition of close neighbors. The range of electrical potential was related to the Debye length (κ^{-1}) or the screening length, which is the distance from the particle surface over which the electrical potential falls to $1/e$ (0.368) of its surface potential.[18] It can be calculated by

$$k^{-1} = \sqrt{\frac{\varepsilon\varepsilon_0 kT}{2e^2 z^2 n_\infty}} \tag{2}$$

where ε is the dielectric constant of the medium (80.1), ε_0 is the permittivity of free space, k is the Boltzmann constant, T is the

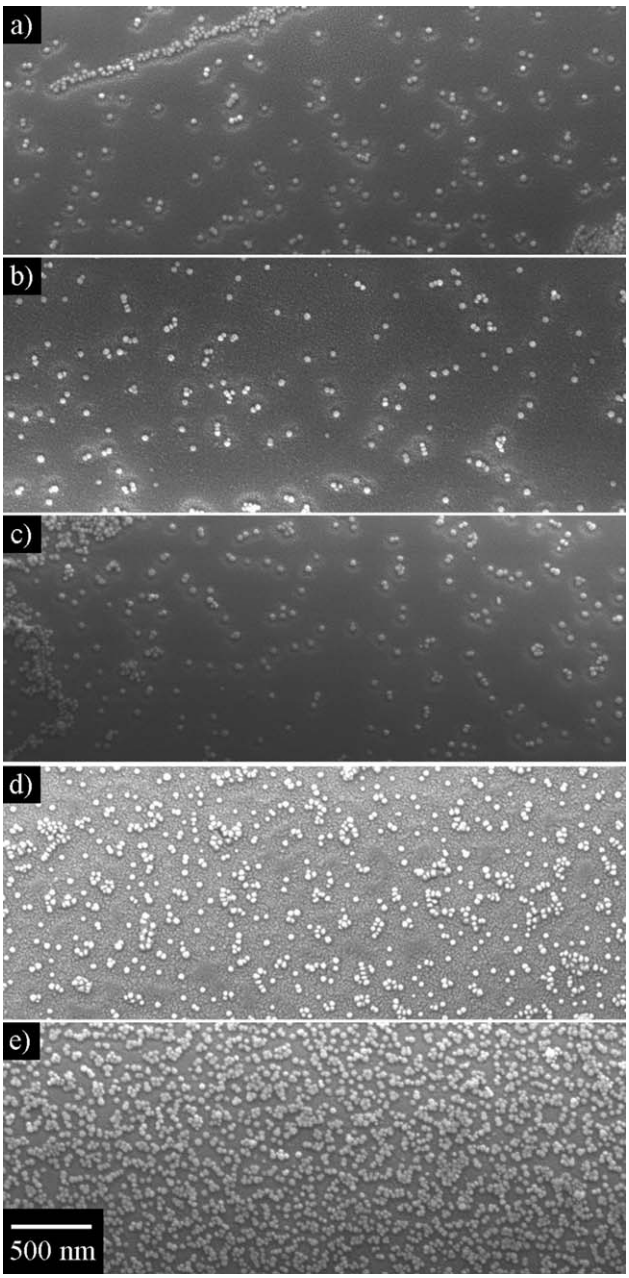

Figure 2. Change in the surface coverage of SPEI-functionalized, 26-nm silica particles on GPS-functionalized fibers with KNO_3 concentrations of (a) 0, (b) 0.01, (c) 0.05, (d) 0.25, and (e) 0.75*M*.

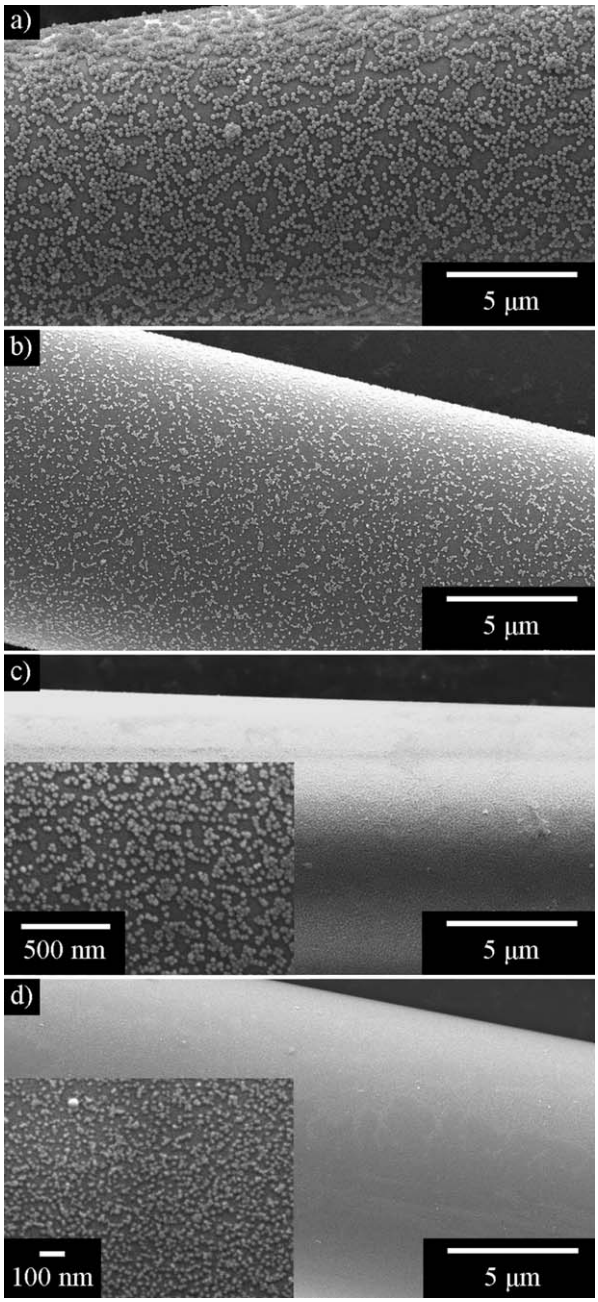

Figure 3. SEM micrographs of GPS glass fibers with (a) 100-, (b) 71-, (c) 26-, and (d) 16-nm SPEI particles deposited on the surface with KNO_3 concentrations of 0.5, 0.75, 0.015, and 0.05*M*, respectively.

temperature, e is the protonic charge, z is the valence of the background electrolyte (1–1), and n_∞ is the number density of the electrolyte (Avogadro's constant, or the molarity of the solution divided by 1000, or 4.5×10^{20} molecules/L for 0.75*M*). Thus, by the addition of an electrolyte, such as KNO_3, the range of electrostatic repulsion can be reduced. KNO_3 was chosen as an electrolyte because neither ion specifically adsorbed to the fiber or particle surfaces.[19]

The optimum salt concentration was determined for each particle size by systematic variation of the concentration, the coating of GPS-functionalized fibers, and observations with SEM. An example of the surface coverage dependence on the electrolyte concentration is shown in Figure 2, where the KNO_3 concentration was varied from 0 to 0.75*M* for the colloidal suspension of 26-nm functionalized particles. Example micrographs of the particle coating for each particle size, 16, 26, 71, and 100 nm, with 0.5, 0.75, 0.015, and 0.05*M* KNO_3, respectively, are shown in Figure 3. For the two smallest particle sizes, the amount of electrolyte needed to achieve targeted surface coverage was much larger than anticipated. We postulated that the volume of the electrical double layer, that is, the region surrounding the charged particles with an elevated concentration of electrolyte and caused by the electrostatic attraction of counterions, was

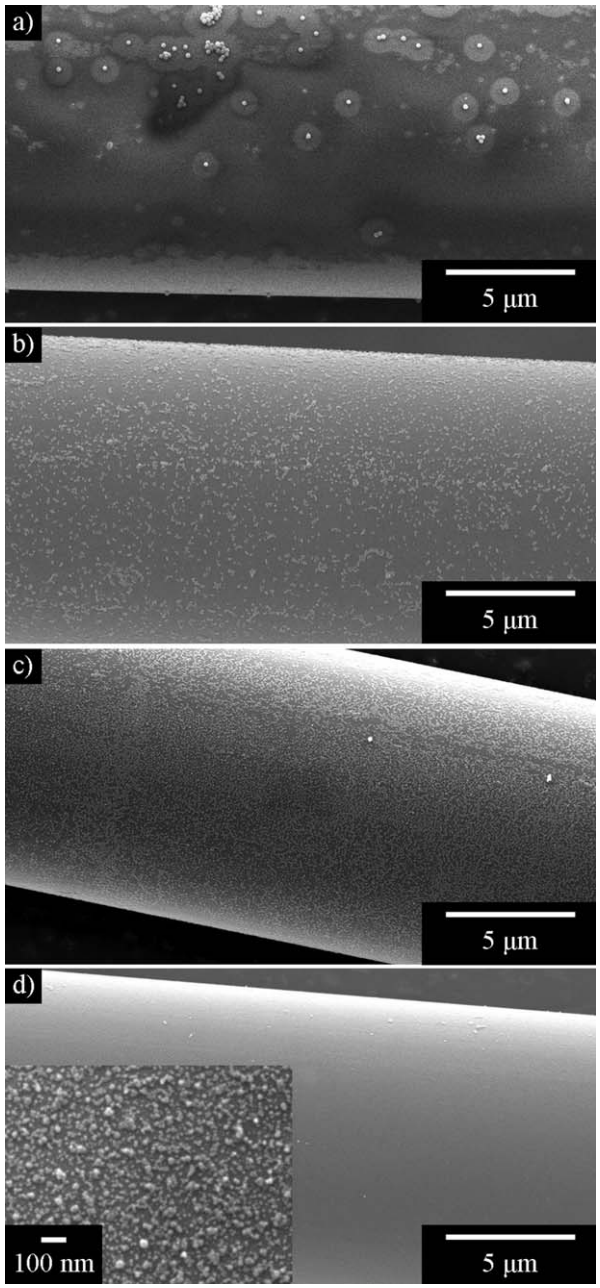

Figure 4. SEM micrographs of the GPS glass fibers with (a) 100-, (b) 71-, (c) 26-, and (d) 16-nm SPEI particles following the wipe test.

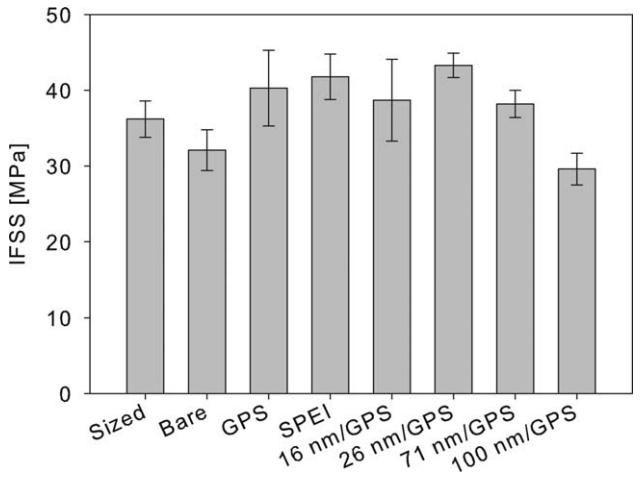

Figure 5. IFSS for the sized (as-received), bare (desized), GPS-functionalized, SPEI-functionalized, and GPS-functionalized fibers with 16-, 26-, 71-, and 100-nm SPEI-functionalized particles, respectively.

sufficient to cause depletion of the bulk electrolyte concentration; this necessitated large amounts of KNO_3.

Wipe Test

The wipe test qualitatively revealed the effect of the particle size on the particle–fiber adhesion. The particle–fiber adhesion was dependent on the ratio of the bonded area to height, or more precisely, the ratio of the strength of the particle–fiber bond to the amount of force exerted by the filter paper. Additionally, smaller functionalized particles were composed of proportionally more SPEI than the larger particles because they had a larger surface area per unit mass. This was confirmed with TGA; we found that functionalized 16-, 26-, 71-, and 100-nm silica particles contained 57, 28, 1.9. and 0.3 wt % polymer, respectively. Because SPEI was essential for adhesion between the particles and fibers, larger amounts improved the adhesion. SEM micrographs of the fiber surfaces, after the wipe test of the four particle systems tested, are shown in Figure 4. The 100-nm particles were almost completely removed from the fiber surface, whereas the 16-nm particles appeared to be unaffected. The 71- and 26-nm particles showed intermediate degrees of particle removal from the wipe test. These results had implications on the effect of the particles on the IFSS, as the particles needed to be well adhered to provide mechanical interlocking between the fiber and the matrix. This test was also used to screen other surface chemistries that are not discussed here.

IFSS

The deposition of SPEI-functionalized silica nanoparticles onto the surface of E-glass fibers altered the fracture toughness of the interphase and improved shear stress transfer via mechanical interlocking between the particles and the matrix when the particles were sufficiently well adhered to the fiber surface. There was no attempt to quantitatively determine the individual contributions of these different mechanisms to IFSS.

IFSS has been used extensively to determine the adhesion between a fiber and matrix with much success. An aspect of the test that is often overlooked is the effect of the growth of debonded regions near fiber breaks as the applied strain is increased. These debonded zones can cover much of the fiber and can transfer shear stress by friction, albeit less effectively.[20,21] The size of these debonded regions is dictated by the fracture toughness of the interface.[22,23]

The ability of the interphase to transfer stress from the polymer matrix to the glass fiber was determined by SFFTs.[1,23,24] When a tensile strain was applied to the dogbone specimen, load was transferred to the fiber by shear stress at the fiber surface. With increasing strain, the fiber axial tensile stress increased until the strength of the fiber was exceeded; this caused the fiber to break. Additional strain was applied, and the process continued until the area of the fiber fragment was too small to transfer sufficient stress to cause further fiber breaks. This l_c was used to estimate IFSS with eq. (1) and was taken to be 4/3 of the average segment length. The IFSS for the as-received, bare (desized), GPS-functionalized, SPEI-functionalized, and GPS-functionalized fibers with 16-, 26-, 71-, and 100-nm SPEI-functionalized particles are shown in Figure 5.

The removal of the sizing decreased the IFSS by 11% because the adhesion promoters present in the sizing were removed. The treatment of the bare fibers with GPS increased the IFSS by 26%. When the GPS was added to the ethanol–water mixture, the alkoxyl groups were hydrolyzed and formed a silanol. This silanol then underwent condensation reactions with the hydroxyl groups of the fiber surface and other silanol in solution and on the fiber surface to form a partially crosslinked silane network.[25] When the single-fiber composites were made, the epoxide functionality in the silane network could covalently bond to the amine groups of the mPDA curing agent to form a crosslinked interphase between the fiber and the matrix; this increased IFSS.

The SPEI functionalization increased IFSS by 30%; this was similar to the increase seen with GPS, as it also covalently bonded to both the fiber and matrix. This was fortuitous because changes in IFSS in the systems with SPEI-functionalized particles were attributed to the addition of particles to the interphase, not simply to a change in the surface chemistry. The precise structure of SPEI on the fiber surface was not as well understood as that of GPS. The level of crosslinking via silanol condensation reactions was likely reduced, from the steric hindrance of the relatively large molecular weight of the PEI. Additionally, acid–base complexes were formed between the hydroxyl groups on the fiber surface and the amines of the SPEI; this provided an alternate mechanism of functionalization. Regardless, SPEI was shown to be an effective adhesion promoter between the glass fibers and the EP-828/mPDA matrix.

The 26-nm SPEI-functionalized silica particles on the GPS-functionalized fibers increased the IFSS by 35% over that of the bare fibers and 8% over that of the GPS fibers (with $p = 0.022$ according to a two-tailed, heteroscedastic t test) with no particles. This improvement was attributed to an increase in the fracture toughness and mechanical interlocking between the particle layer and the matrix,[26] which improved adhesion. The 26-nm functionalized particles were well adhered to the fiber surface, as demonstrated by the wipe test; this allowed for improved shear stress transfer by mechanical interlocking. When the fracture toughness was increased and fiber debonding

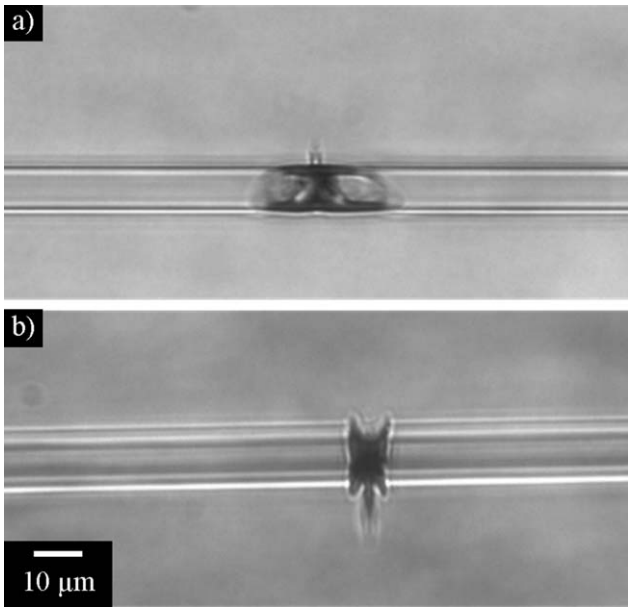

Figure 6. Optical micrographs of GPS fibers (a) without a particle-modified interphase and (b) with a 26-nm SPEI-functionalized particle-modified interphase.

was prevented, the entire fiber remained bound to the matrix; this allowed for optimum shear stress transfer as the SFFT proceeded. This was illustrated with transmitted light microscopy.

Transmitted, visible light microscopy images were taken of the fiber ends, after an SFFT. The images permitted qualitative assessment of the adhesive strength between the fiber and matrix.[27] An example, showing the fiber ends of the GPS fibers and GPS fibers with 26-nm SPEI particles, is shown in Figure 6.

A debonded region near the fiber end on a GPS-functionalized fiber is shown in Figure 6(a). The addition of 26-nm SPEI-functionalized particles to the interphase increased the adhesion between the fiber and matrix and prevented debonding, as shown in Figure 6(b). Optical micrographs were taken of all of the systems studied. The systems with a low IFSS showed large debonded regions, whereas systems with a high IFSS showed less or no debonding.

The increase in the fracture toughness was further investigated by SEM observations of the fracture surfaces of high fiber volume fraction (V_f) composites made with the four particle sizes investigated fractured in the fiber direction via mode I crack growth, as shown in Figure 7. The 26-nm particles [Figure 7(c)] generated a fracture surface with observable roughness (right side of the image) and, in some locations, cohesive failure (left side of the image). This was in contrast to the smooth, adhesive failure between the bare and GPS-functionalized fibers and the matrix.

The 16-nm particles, on average, decreased the IFSS by 4% compared to that of the GPS-functionalized fibers, but this difference was not statically significant ($p = 0.359$). These particles were too small to provide a significant amount of shear stress transfer by mechanical interlocking. Thus, the 16-nm particles were too small to significantly affect IFSS. The toughening mechanisms observed with the 26-nm particle samples via SEM were not observed with the 16-nm particles, shown in Figure 7(d). The fiber surfaces appeared to be smooth because the crack grew at the particle–matrix interface, and the particles were too small to significantly increase the surface roughness.

The 71- and 100-nm particles decreased the IFSS by 4 and 27%, respectively, when compared to GPS-functionalized fibers

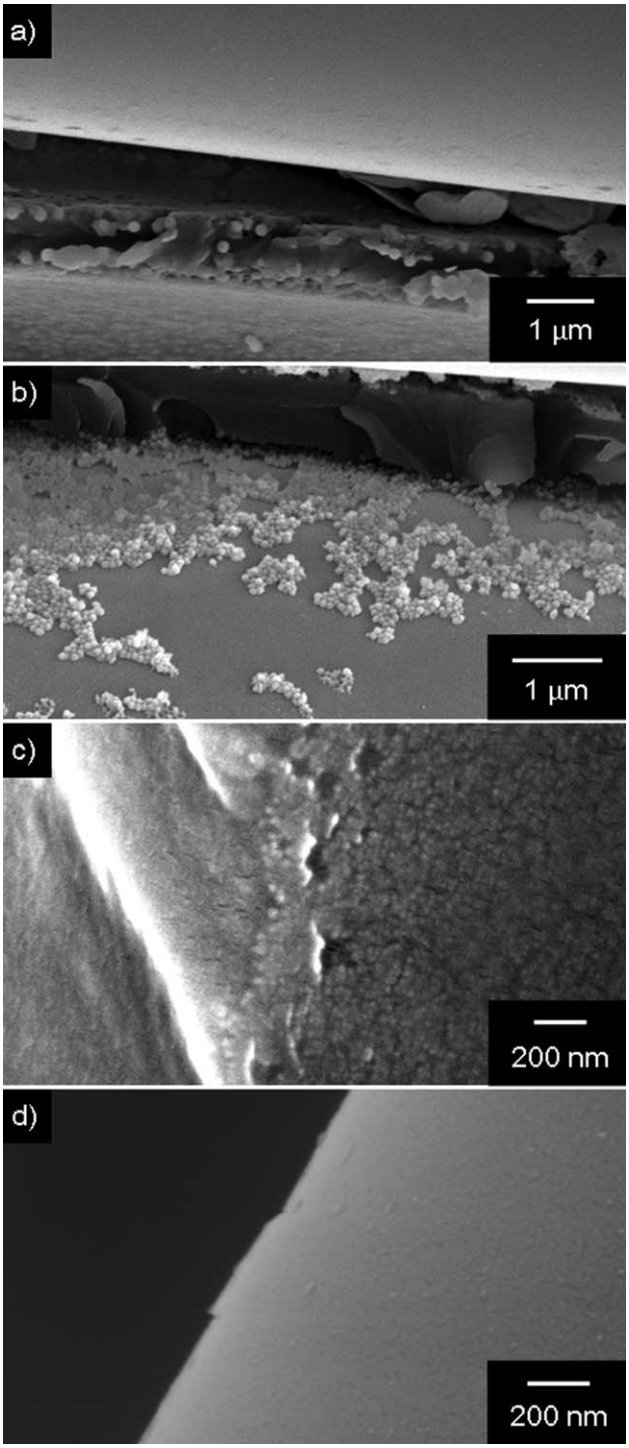

Figure 7. Mode I fracture surface of a unidirectional high-V_f composite with fibers treated with (a) 100-, (b) 71-, (c) 26-, and (d) 16-nm SPEI particles.

($p = 0.051$ and 0.000, respectively). These larger particles were not well adhered for the level of shear force applied between the fiber and particles; this prevented effective mechanical interlocking and interfered with the adhesion of the matrix to the fiber. This led to decreases in IFSS. The SEM of the fracture surfaces showed that the 100-nm particles remained entirely embedded in the matrix (bottom); this left a smooth fiber surface [top; Figure 7(a)]. The 71-nm particles [Figure 7(b)] were an intermediate case; many particles remained adhered to the fiber surface (bottom), whereas many were removed with the matrix.

The SPEI-functionalized 26-nm particles were also deposited on the sized and bare fibers. The IFSS values of these systems and the same fiber functionalizations without particles are shown in Figure 8. The deposition of functionalized 26-nm particles on the sized and bare fibers increased IFSS by 16% ($p = 0.001$) in both cases. This indicated that the use of appropriately sized particles could be a robust method for improving IFSS, even when they are applied after the application of sizing.

Transverse Flexural Strengths of the Unidirectional Composites

Most specimens had V_f's of 0.65 ± 0.01, with the exception of the fibers treated with 71- and 100-nm particles, which had V_fs of 0.61 and 0.73, respectively.

The results of the three-point bending test were largely similar to those of SFFT. There was a 93% increase in the flexural strength when the desized fibers were treated with GPS. The deposition of 16- and 26-nm particles on the surface of the GPS-functionalized fibers did not cause a statistically significant change in the flexural strength ($p = 0.52$ and 0.59, respectively). Increasing the particle size further decreased the flexural strength, as the particles were relatively poorly adhered, and this reduced the adhesive strength in the composite. The flexural strength and modulus results are shown in Figure 9. The flexural modulus did not change with fiber surface treatment, as was expected. The system with 71-nm particles deposited on the surface had a slightly lower modulus because it had a slightly lower V_f than the other samples.

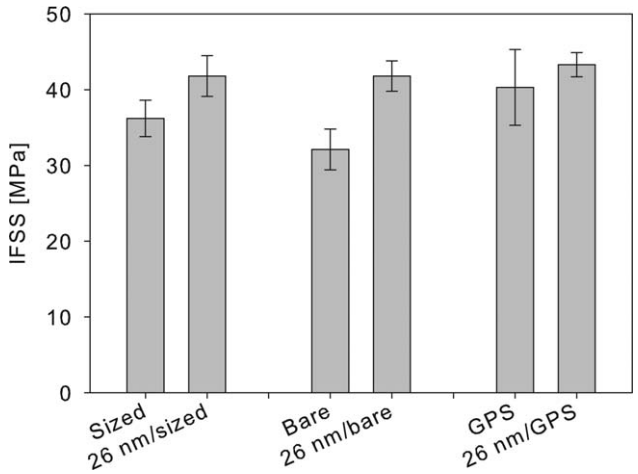

Figure 8. IFSS values of the sized, bare, and GPS-functionalized E-glass fibers with and without SPEI-functionalized 26-nm silica particles.

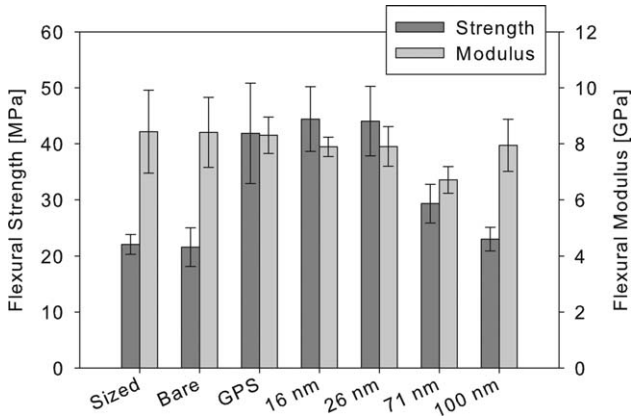

Figure 9. Transverse flexural strength and modulus of a unidirectional composite made with various fiber surface treatments; dark gray indicates the strength, and light gray indicates the modulus.

CONCLUSIONS

Uniform, dense coverage of the SPEI-functionalized silica nanoparticles on the E-glass fiber surfaces was achieved by careful control of the electrostatics of the deposition process. The pH was adjusted to 7 to achieve a strong negative surface charge on the fibers and a strong positive surface charge on the functionalized particles. Various amounts of KNO_3 were added to reduce the range of electrostatic repulsion between the particles; this increased the surface coverage on the fibers and led to uniform, near monolayer coverage.

The size of the functionalized silica nanoparticles deposited onto the E-glass fibers played an important role in the level of adhesion between the fibers and the matrix of mPDA and BADGE epoxy, EP-828. When functionalized 26-nm particles were used on a GPS-functionalized fiber, IFSS was increased by 35% over the bare fibers and 8% over the GPS-functionalized fibers. These particles were well adhered to the fiber surface; this provided an increase in the mechanical interlocking and fracture toughness. Smaller particles (16 nm) were also well adhered, but they were too small to significantly increase the surface roughness. Thus, this provided no increase in the mechanical interlocking or fracture toughness, so the IFSS was unchanged. Larger particles (71 and 100 nm) had a relatively low ratio of particle–fiber contact area to height and were thus poorly adhered; this caused fiber–matrix debonding and poor stress transfer from the matrix to the fiber in the SFFT and resulted in a reduced IFSS values and failure at the fiber–particle interface in the three-point bending test.

ACKNOWLEDGMENTS

The authors gratefully acknowledge financial support from Toray Composites (America), Felix Nguyen for helpful discussions, and Jeff Richards for insight on the use of salt to control nanoparticle deposition.

REFERENCES

1. Herrera-Franco, P.; Drzal, L. *Composites* **1992**, *23*, 2.
2. Madhukar, M.; Drzal, L. *J. Compos. Mater.* **1991**, *25*, 958.

3. Leonard, G. C.; Hosseinpour, D.; Berg, J. C. *J. Adhes. Sci. Technol.* **2009**, *23*, 2031.
4. Plueddemann, E. Silane Coupling Agents; Plenum: New York, **1982**.
5. Rabotnov, J. N.; Perov, B. V.; Ssorina, T. G.; Stepanitsov, E. I. *Plast. Inst. Proc.* **1974**, *65*.
6. Thostenson, E. T.; Li, W. Z.; Wang, D. Z.; Ren, Z. F.; Chou, T. W. *J. Appl. Phys.* **2002**, *91*, 6034.
7. Zhao, Z. G.; Ci, L. J.; Cheng, H. M.; Bai, J. B. *Carbon* **2005**, *43*, 663.
8. Lin, Y.; Ehlert, G.; Sodano, H. A. *Adv. Funct. Mater.* **2009**, *19*, 2654.
9. Ehlert, G. J.; Sodano, H. *ACS Appl. Mater. Interfaces* **2009**, *1*, 1827.
10. Galan, U.; Lin, Y.; Ehlert, G. J.; Sodano, H. *Compos. Sci. Technol.* **2011**, *71*, 946.
11. Gao, X.; Jensen, R. E.; Li, W.; Deitzel, J.; McKnight, S. H.; Gillespie, J. W. *J. Compos. Mater.* **2008**, *42*, 513.
12. Bekyarova, E.; Thostenson, E. T.; Yu, A.; Kim, H.; Gao, J.; Tang, J.; Hahn, H. T.; Chou, T.-W.; Itkis, M. E.; Haddon, R. C. *Langmuir* **2007**, *23*, 3970.
13. Kamae, T.; Drzal, L. T. *Compos. A* **2012**, *43*, 1569.
14. Jensen, R.; McKnight, S. *Compos. Sci. Technol.* **2006**, *66*, 509.
15. Gao, X.; Jensen, R. E.; McKnight, S. H.; Gillespie, J. W. *Compos. A* **2011**, *42*, 1738.
16. Kelly, A.; Tyson, W. *J. Mech. Phys. Solids* **1965**, *13*, 329.
17. Zinck, P.; Mader, E.; Gerard, J. F. *J. Mater. Sci.* **2001**, *36*, 5245.
18. Berg, J. C. An Introduction to Interfaces & Colloids: The Bridge to Nanoscience; World Scientific: Singapore, **2010**; p 471.
19. Hunter, R. J. Foundations of Colloid Science; 2nd ed.; Oxford University Press: Oxford, United Kingdom, **2001**; pp 313 and 336.
20. Feillard, P.; Desarmot, G.; Favre, J. P. *Compos. Sci. Technol.* **1994**, *50*, 265.
21. Copponnex, T. *J. Compos. Sci. Technol.* **1996**, *56*, 893.
22. Ramirez, F. A.; Carlsson, L. A.; Acha, B. A. *Compos. A* **2009**, *40*, 679.
23. Kim, J. K.; Mai, Y. W. Engineered Interfaces in Fiber Reinforced Composites; Elsevier Science: Amsterdam, **1998**.
24. Feih, S.; Wonsyld, K.; Minzari, D.; Westermann, P.; Lilholt, H. Testing Procedure for the Single Fiber Fragmentation Test; Risø-R-1483(EN); Risø National Laboratory: Roskilde, Denmark, **2004**; p 30.
25. Iglesias, J. G.; González-Benito, J.; Aznar, A. J.; Bravo, J.; Baselga, J. *J. Colloid Interface Sci.* **2002**, *250*, 251.
26. Packham, D. *Int. J. Adhes. Adhes.* **2003**, *23*, 437.
27. Drzal, L. T. *Vacuum* **1990**, *41*, 1615.